Regular Article – Atomic and Molecular Collisions

Electron impact partial ionization cross sections of 1-butanol

Kanupriya Goswami[1,a] , Meetu Luthra[2] , Ajay Kumar Arora[1] , Anand Bharadvaja[2,b] , and Kasturi Lal Baluja[3]

[1] Department of Physics, Keshav Mahavidyalaya, University of Delhi, Delhi 110034, India
[2] Department of Physics, Bhaskaracharya College of Applied Sciences, University of Delhi, New Delhi 110075, India
[3] Department of Physics and Astrophysics, University of Delhi, Delhi 110007, India

Abstract. The 1-butanol molecule is one of the most promising sources of biofuel, having the potential to replace fossil fuels. It can be used in combustion engines as fuel. During the combustion, plasma is created in which the electron interactions with neutral targets result in the formation of cations via dissociative ionization process. The energy-dependent cross sections are reported for different cations up to 5 keV in a very simple and efficient way within the framework of the binary-encounter model. The computation approach requires the binary-encounter-Bethe input parameters, ion energetics, and electron ionization mass spectrometry data. A good agreement is observed between the computed cross sections and experimental measurements for various cations. The work emphasizes the role of electron mass spectrometry in the study of the ionization process. The electron collision data would be useful to model the combustion process to develop efficient combustion engines. The present work provides the only available theoretical results for 1-butanol over an extensive energy range.

1 Introduction

Alcohols are considered as the potential energy source capable of mitigating the energy crisis, providing a clean environment, and also helping in conserving natural resources. They are also regarded as the alternative fuels for low-temperature combustion in internal combustion engine applications. Being oxygenated, the alcohols burn faster and release minimal levels of CO_2 and unburnt hydrocarbons in the atmosphere than conventional fossil fuels. Even the amount of CO_2 released from the burning of alcohol fuels can be recycled by plants through the photosynthesis process that is used to produce alcohol fuels. Alcohols as biofuels can be produced from renewable, and biomass sources [1,2]. 1-butanol or butanol has superior physicochemical properties [3,4] and good blending properties than several primary alkane alcohols. It has fuel properties closer to

the diesel fuel [5] and can mix easily with petroleum fuels, thus reducing soot emissions, greenhouse gases, and other pollutants [6–8]. This makes butanol an excellent candidate for being used in conventional combustion engines [4,9].

Butanol can be produced from biomass [10,11], oilseeds [12], and other renewable resources [3,4,13]. Apart from being used as biofuel, it is also used in chemical industries [14].

The electron-induced ionization initiates the chemical processes in the spark plugs of the internal combustion engines. The plasma is created during the combustion process which consists of electrons, molecules, ions, and atoms. The ions act as additives to fossil fuels and thus increase the combustion rate [15] by decreasing the ignition delay times [16]. The formation rate of these species is related to their respective cross sections. The collision data are useful to improve the performance of internal combustion engines [17,18] and for the better understanding of the combustion process [19,20]. The kinetic-chemical models used in spark-ignited engines [21–24], plasma-assisted combustion [25–31] and in plasma simulation codes [32–34] require electron–molecule cross section data of the species present and created in the plasma.

The study of electron impact ionization and dissociative ionization of molecules is fundamental, interdisciplinary and of technological relevance [35–39]. The electron ionization molecular beam mass spectroscopy

Kasturi Lal Baluja: Formerly at Department of Physics and Astrophysics, University of Delhi, Delhi, 110007, India. Ajay Kumar Arora is on leave from his parent institution Keshav Mahavidyalaya.

Supplementary Information The online version contains supplementary material available at https://doi.org/10.1140/epjd/s10053-022-00425-3.

[a] e-mail: kanupriyagoswami@keshav.du.ac.in

[b] e-mail: anand_bharadvaja@yahoo.com (corresponding author)

[40] is frequently used to study combustion chemistry of biofuels [22,41], hydrocarbons [42], and ions [43]. The electron impact ionization cross sections are required to model plasma processes occurring in environments like cometary and planetary atmospheres, astrophysics, radiation physics, plasma electronics, etc. [44–53]. Although the electron interactions are relatively well studied for butanol [19,54], the data on partial ionization cross sections (PICS) are scarce.

Ghosh et al. have determined the mass spectrum of cations produced due to ionization of butanol by electrons at 70 eV [55]. Pires et al. have measured the individual PICS for several cations using a Hiden Analytical quadrupole mass spectrometer from 10 to 100 eV energy range [56]. Zavilopulo et al. have measured the mass spectra, and ionization functions for several primary alcohols, including butanol [57]. These authors carried out the experiment with the help of a monopole mass spectrometer using crossed electron and molecular beam methods.

The quantum mechanical modeling of the ionization process involves the use of a large basis set, solving a large number of coupled equations, and inter-channel coupling between the bound and continuum states [58–60]. This complicates the computation of total ionization cross sections (TICS) and also makes the calculations expensive due to enormous computational resources involved [61–63]. The multicenter nature of molecules makes the ab initio methods challenging to apply to heavier molecules. Butanol is a complex molecule with having a significantly large number of atoms. The use of ab initio methods like the molecular convergent close-coupling (MCCC) [62] would require significant computational resources and may still make the scattering calculations intractable. So far, the MCCC methods have only been applied to lighter diatomic molecules [63,64]. The semiempirical approach-based modified-binary-encounter-Bethe model has successfully been used to model the dissociative ionization phenomenon [65–68]. This modified-BEB model, just like the binary-encounter-Bethe (BEB) model, does not require any knowledge of fitting parameters, wavefunction, and differential oscillator strengths. It requires the BEB model input parameters and additional inputs like ion energetics and the mass spectrometry (MS) data. This makes the modified-BEB model simpler to use in comparison to the modified Jain-Khare [69] which involves the use of differential oscillator strengths. Although the differential oscillator strengths can be extracted from photoionization cross section data, the computation of photoionization is a tedious task.

In this work, we have computed the PICS of cations created during dissociative ionization of butanol using the modified-BEB model [66–68] for electron energies up to 5 keV. The computed PICS show a remarkable agreement with the experimental results for the majority of cations. The work shows that PICS can be calculated without any difficulty using the modified-BEB (m-BEB) approach for any complex molecule. It also highlights the importance of mass spectrometry data

in the study of the dissociative ionization process. The paper is organized as follows. In Sect. 2, we present a methodology to compute partial ionization cross sections and results. The conclusion is drawn in Sect. 3.

2 Method and details: the BEB model

In the BEB model, the total electron impact ionization cross section is the sum of cross sections per molecular orbital i [70].

$$Q^I(t) = \sum_i \frac{S_i}{t_i + u_i + 1} \left[\frac{1}{2} \left(1 - \frac{1}{t_i^2} \right) \ln t_i \right. $$
$$\left. + 1 - \frac{1}{t_i} - \frac{\ln t_i}{t_i + 1} \right] \qquad (1)$$

where $t_i = E/|B_i|$; $u_i = U_i/|B_i|$; $S = 4\pi a_0^2 N_i (R/|B_i|)^2$.

The notations $|B_i|$ and U_i represent the magnitude of the binding and orbital kinetic energies of the ith orbital, respectively. E is the incident energy of the projectile, R is a Rydberg constant, and a_0 is the Bohr's radius. N_i denotes the number of electrons in ith orbital. At high incident electron energies, a relativistic version of BEB may be appropriate to compute TICS [71]. This BEB formula in its present form cannot model the dissociative ionization process. To obtain the PICS of cations formed during ionization, equation (1) is modified by : (a) The ionization energy (IE) of the precursor molecule is replaced by the appearance energy (AE) of a cation. It is because the appearance of energy characterizes the ion. In the BEB model, the magnitude of the binding energy of the highest occupied molecular orbital (HOMO) represents the molecule's IE. To use the input parameters of the molecule to compute PICS for cations, a transformation in $|B|$ is required so that each ion is represented by correct threshold behavior in cross section data. This is done by incrementing the binding energy of the molecular orbital by an amount equal to the difference between the appearance energy of a fragment and absolute value of binding energy, *i.e.*, the first ionization energy of the neutral target. Thus, $|B| \rightarrow |B| + \Delta_j$ where $\Delta_j = AE_j - |B|$, $|B| + \Delta_j$ becomes the AE of HOMO of a particular fragment in BEB model for cations.

(b) Scaling the partial cross sections of a cation by a factor Γ to ensure that the branching ratio (BR) obtained from the modified-BEB model for each fragment is normalized to their corresponding experimental values. Thus, Γ corrects the amplitude of the curve for each fragment j without disturbing the validity of the Born approximation at high energy. The experimental value of BR are obtained from the electron ionization mass spectrometry data and are calculated at the energy at which the mass spectrum is recorded.

Thus, for the fragment j, $t_j = E/AE_j$ and $AE_j = |B| + \Delta_j$. The normalized PICS for a fragment j after incorporating above modifications and summing

over the molecular orbitals i are given by :

$$Q'_j (t) = \Gamma_j \sum_i \frac{S_{ji}}{t_{ji} + u_{ji} + 1} \left[\frac{1}{2} \left(1 - \frac{1}{t_{ji}^2} \right) \ln t_{ji} \right.$$
$$\left. + 1 - \frac{1}{t_{ji}} - \frac{\ln t_{ji}}{t_{ji} + 1} \right]. \qquad (2)$$

In the modified-BEB equation (2), $u_{ji} = U_i/t_{ij}$ and $S_{ji} = 4\pi a_0^2 N_i (R/t_{ij})^2$.

The BEB model, ever-since it was proposed by Kim and Rudd (1994), has undergone several modifications as summarized in reference [67]. The m-BEB or modified-BEB model in the present study refers to the computation of PICS by suitably modifying the BEB model of Kim and Rudd [70]. We have used this nomenclature here as well as in earlier [66–68].

2.1 Computational details

The molecule was optimized at Hartree–Fock level using a 6-311G* basis set. This was done using the Gaussian 03 software [72]. The reaction energetics data of different cations were referred from the experimental work of Ghosh et al. [55]. These authors had determined the AEs by employing a nonlinear fitting of the Wannier threshold law, by fitting the relevant cation intensity data of counts versus impact energy E, at energies near to the threshold. Although the value B for occupied orbital was determined from Gaussian 03 software, the experimental values of AE were preferred. It is because the outermost valence orbital dominates the ionization cross section. Also, the use of the experimental value

of AE gives the correct threshold behavior of cross sections. However, for inner orbitals, the theoretical value of B was used. The mass spectrometry data reported by Pires et al. [56] were used to determine the BR at electron energy of 70 eV. Thus, the branching ratios calculated from mass spectrometry data are at only one energy (70 eV). The electron impact ionization (EI) of butanol results in a total of 76 cations [55]. The j therefore, varies from 1 to 76. The apparent limitations of the model are discussed at the end.

The relative intensity of cations, their AE and the BRs are shown in Table 1.

2.2 Results and discussion

The mass spectrum of butanol reported by Pires et al. [56], NIST Chemistry WebBook [73], Zavilopulo et al. [57] and Friedel et al. [74] are consistent with each other. However, the number of fragmented cations reported by Pires et al. [56] is far more than the other authors. For this very reason, we have referred to the spectrometry data of Pires et al. [56] for computing the PICS.

Pires et al. [56] used a quadrupole mass spectrometer, having an energy resolution of about 0.8 eV and mass resolution of 1 amu. Only the singly ionized ions were identified at 70 eV mass spectrum. The relative abundances of the cations were determined with respect to the base peak of CH_2OH^+ having nominal mass 31 amu. Nearly 56% of the total ion intensity recorded in the mass spectrum is represented by cations having nominal masses 31 amu, 41 amu, 43 amu, and 56 amu. This means that collectively these cations contribute about 56% to TICS.

Table 1 Branching ratios, appearance energies, relative intensities (RI, in %) and scaling factors (Γ) of singly ionized cations generated by EI of 1-butanol at 70 eV

m/z	RI [56]	AE (eV) [55])	BR	Γ	m/z	RI [56]	AE (eV) [55]	BR	Γ	m/z	RI [56]	AE (eV) [55]	BR	Γ
1	1.58	–	0.0029	–	31	100	11.76	0.1804	0.266	51	0.75	12.80	0.00135	0.00212
2	1.56	–	0.0028	–	32	5.94	11.09	0.0107	0.0147	52	0.42	–	0.00077	–
3	0.01	–	0.0	–	33	10.28	11.60	0.0185	0.027	53	1.24	12.28	0.00224	0.0034
12	0.12	22.27	0.0002	0.0008	34	0.23	–	0.00042	–	54	1.15	–	0.00207	–
–	–		– –	–	35	0.06	–	0.00011	–	55	14.68	11.61	0.02648	0.0381
14	1.70	15.27	0.0031	0.0063	36	0.07	–	0.00013	–	56	81.93	10.48	0.1478	0.1887
15	7.22	14.56	0.0130	0.025	37	0.85	16.26	0.00154	0.0035	57	5.55	10.56	0.0100	0.0129
16	0.52	–	0.0009	–	38	1.71	13.25	0.0031	0.0052	58	0.17	10.72	0.00034	0.0004
17	1.65	–	0.003	–	39	12.90	10.71	0.0233	0.0305	59	0.33	11.24	0.0006	0.0008
18	6.93	–	0.0125	–	40	5.59	11.52	0.0101	0.0144	60	0.16	10.93	0.00028	0.0004
19	5.69	–	0.0103	–	41	72.78	11.42	0.1313	0.1852	69	0.09	–	0.00016	–
20	–	–	0.0001	–	42	32.60	11.49	0.0588	0.0836	70	0.12	–	0.00022	–
24	0.05	–	0.0	–	43	55.62	11.65	0.1003	0.1449	71	0.13	–	0.00023	–
25	0.32	–	0.00058	0.0017	44	5.44	12.11	0.0098	0.0128	72	0.78	10.12	0.0014	0.0017
26	4.65	11.60	0.0084	0.012	45	5.68	13.16	0.0102	0.015	73	1.39	11.14	0.00251	0.0034
27	43.0	13.63	0.0776	0.1362	46	0.64	11.30	0.00115	0.0016	74	0.73	10.27	0.00132	0.0016
28	27.17	12.34	0.049	0.0759	47	0.11	12.21	0.0002	0.0003					
29	28.6	12.57	0.0517	–	49	0.20	–	0.00036	–					
30	2.03	11.08	0.0037	0.0050	50	0.79	13.12	0.00143	0.0024					

The AE of Ghosh et al. [55] shown in the table is without uncertainties

Like other C_1–C_3 primary alcohols, butanol also shows the maximum ion intensity for the resonance stabilized ion (CH_2OH^+), with mass 31 amu. This cation is formed by the loss of a proton from the carbon atom. The increase in the carbon chain from methanol to 1-propanol (C_1–C_3) results in systematic growth in the production of oxonium ion [56] however, the absolute cross sections for this ion are lower in butanol than 1-propanol [75] and ethanol [76]. This indicates a change in the fragmentation pattern for the most intense ion in butanol. This fragmentation is more spontaneous in butanol and in the higher-order alcohol molecules than C_1 to C_3 alcohols. The different absolute cross sections at 70 eV for the individual oxonium ion of C_1–C_4 alcohols are due to non-identical relative yield estimates. Thus, the BR of oxonium ions for these alcohols is different. The oxonium ion (CH_2OH^+) being the most abundant ion in the mass spectrum of 1-butanol, would have the largest PICS among all other cations and would thus have the maximum contribution to the TICS. This ion contributes about 18% to TICS based on mass spectrometry data. The parent cation $C_4H_{10}O^+$ (m = 74 amu) is formed due to the ejection of an electron from a non-bonding orbital on the oxygen atom and has a small intensity with respect to the base peak. The relative abundances of parent ions of primary alcohols decrease as the carbon chain increases linearly from C_1 to C_4. Since relative abundances are proportional to PICS, it means that the parent ion of the butanol molecule has a smaller ionization cross section than C_1–C_3 primary alcohols. The fragmentation of 1-butanol has been discussed in detail by Pires et al. [56]. In the same work, these authors have measured the absolute PICS only for 38 cations in the energy range 10–100 eV as these cations had the relative abundances higher than 1%. These 38 fragments contributed almost 97% of the total ion abundance in the mass spectra generated by electrons with an impact energy of 70 eV. The cations having masses 65, 67–71, 16–24, 17–18 amu

were excluded in determining the PICS either due to high background contributions, low relative abundance data, or both. The lighter fragments ions like H^+ and H_2^+ were also excluded from measurements.

Two distinct AE thresholds were observed for the cation fragment of mass 50 amu. The PICS were obtained for the cation $C_4H_2^+$ having threshold 10.36 eV. The low abundance (less than 1%) makes this cation susceptible to a contaminant.

The cations represented by masses 53, 50, 45, 44, 41, 29, 28, and 15 amu, were formed through two distinct molecular fragments and thus had identical masses. Few cations (having m/z 55, 53, 52, 41, 29, and 15 amu) had appearance energies either lower or close to the first ionization threshold. These fragments have very low value of relative ion intensity indicating very small PICS and consequently a very minor contribution to the present TICS.

The PICS of different cations obtained using the m-BEB model are displayed in Figs. 1, 2, 3, 4, and 5. The scaling factors required to normalize the cross section data of cations were obtained from the electron ionization mass spectrum data of Pires et al. [56]. The PICS for all cations obtained using the m-BEB approach are smooth and continuous. The m-BEB results are consistent with Pires et al. [56] except for cations with m/z= 12, 13, 14, and 25 amu. These fragments show an increasing trend in experimental cross section data, whereas the theoretical PICS (present results) show a decreasing trend after the peak is attained. In the absence of any structural dependence on PICS [56], it is difficult to assign a particular reason for this variation. Since these cations have very small PICS. This variation would not result in a significant deviation in TICS obtained by summing all the PICS. The peak in cross section for all fragments is around 70 eV. All PICS have thresholds in agreement with the experimental values. However, the disagreement in PICS is largely seen at lower incident energy. It is not surprising, since the
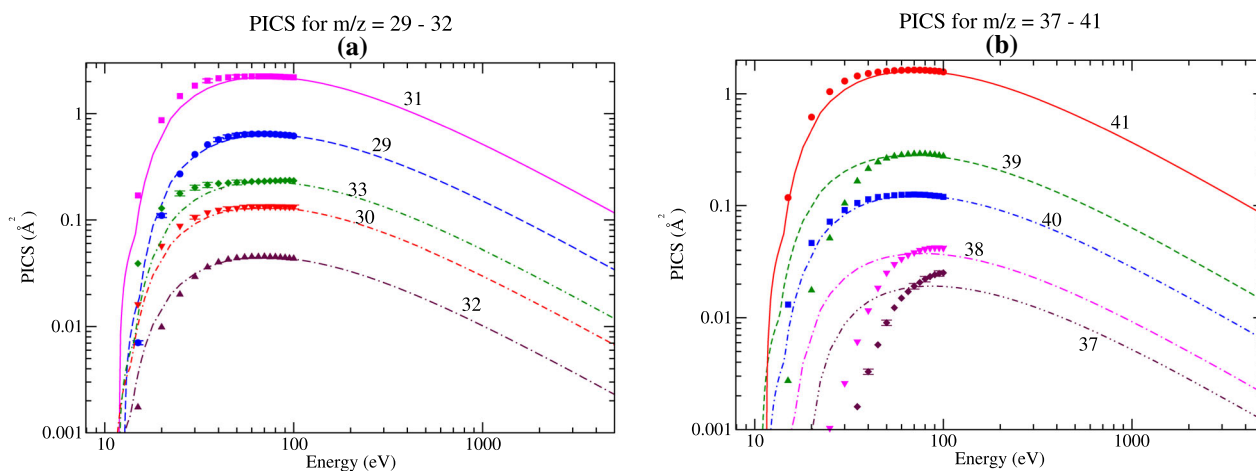

Fig. 1 "(Color online)" Partial ionization cross sections for different fragments. The present theoretical results obtained using m-BEB model are denoted by different line types and the experimental results are denoted by symbols. **a** $m/z =$ 29–32 and **b** $m/z =$ 37–41
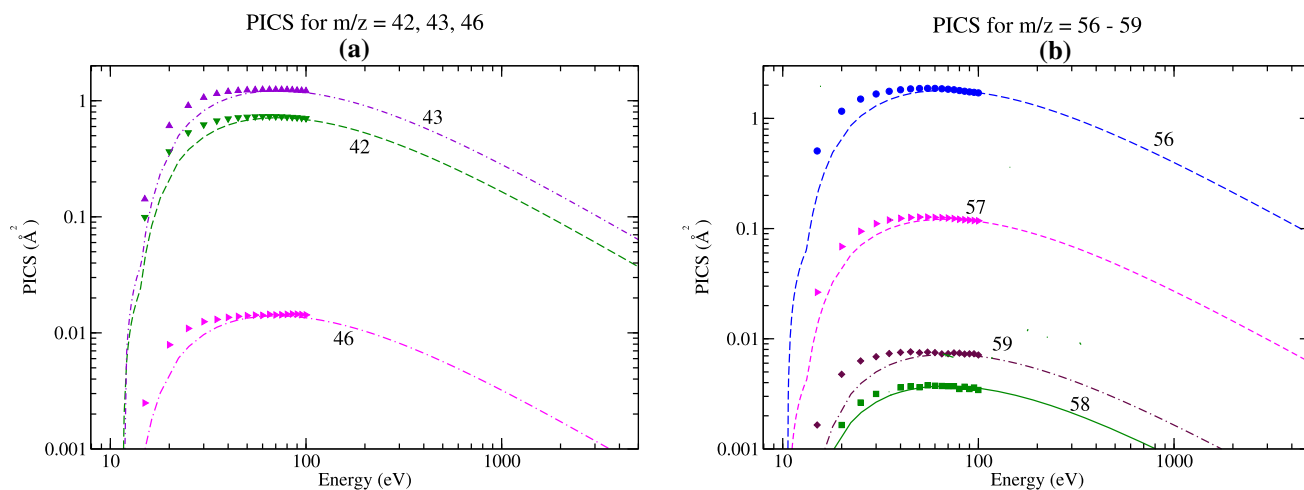
Fig. 2 "(Color online)" Caption same as Fig. 1 but for   **a** $m/z = 42, 43, 46$ and **b** $m/z = 56–59$
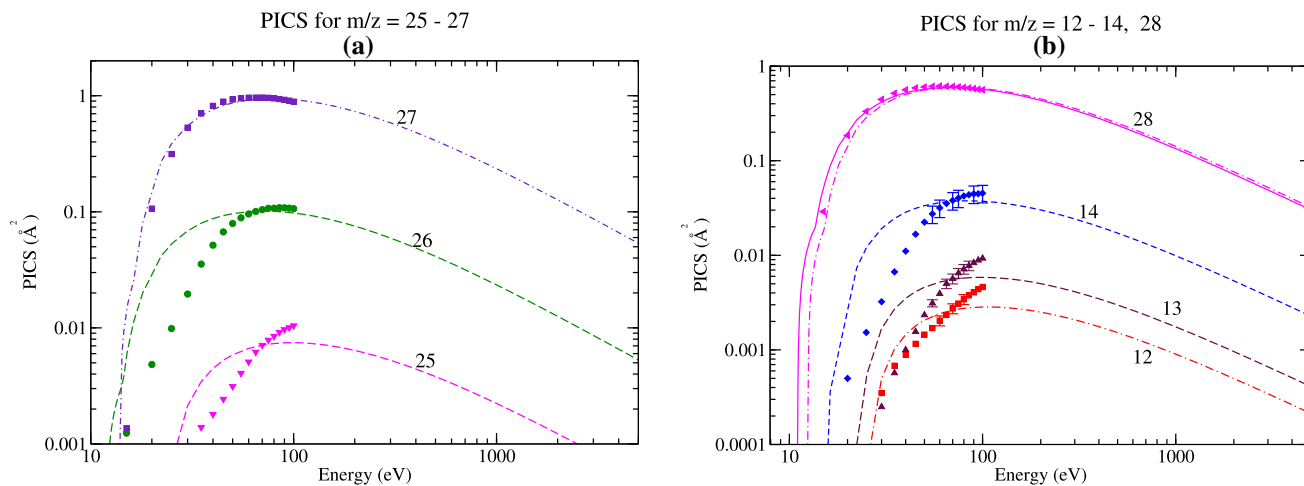

Fig. 3 "(Color online)" Caption same as Fig. 1 but for   **a** $m/z = 25–27$ and   **b** $m/z = 12–14, 28$
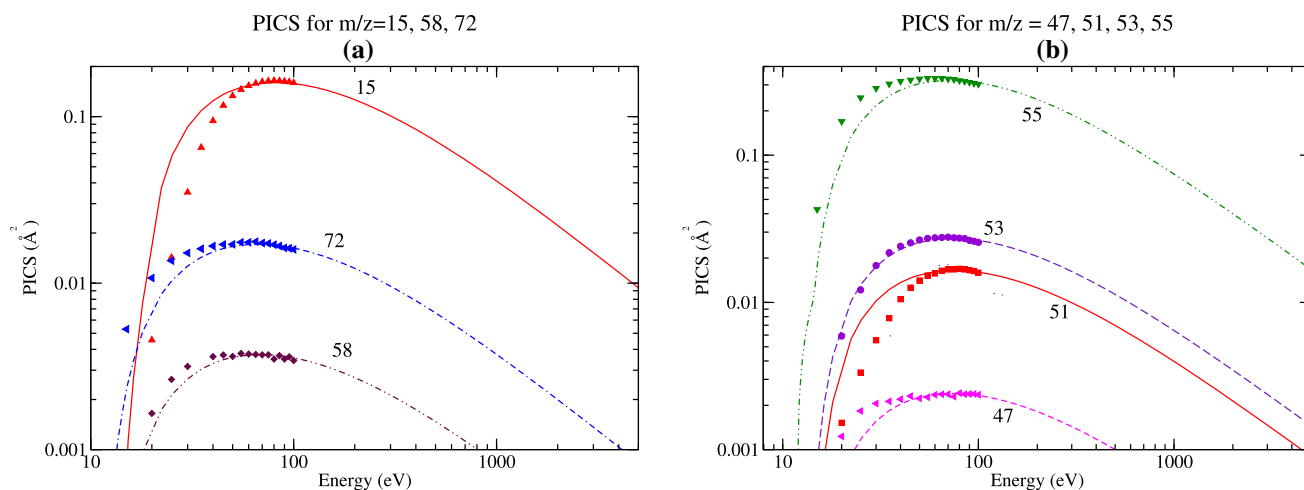

Fig. 4 "(Color online)" Caption same as Fig. 1 but for   **a** $m/z = 15, 58, 72$ and   **b** $m/z = 47, 51, 53, 55$

PICS for m/z = 60, 73, 74
(a)

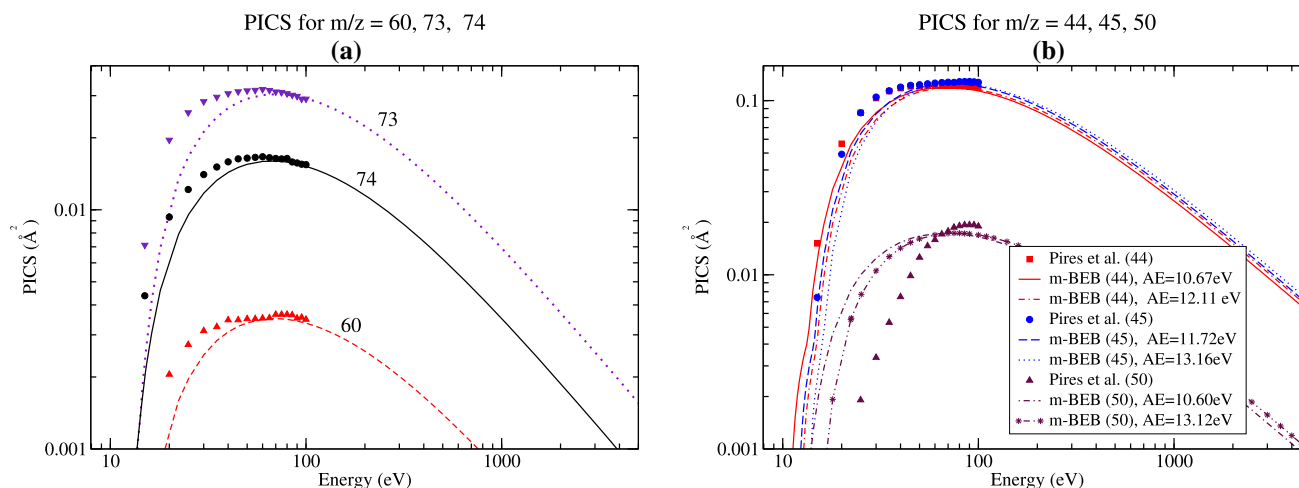PICS for m/z = 44, 45, 50
(b)

Fig. 5 "(Color online)" Caption same as Fig. 1 but for   **a** $m/z = 60, 73, 74$ and **b** $m/z = 44, 45, 50$

BEB model is basically a high energy approximation. It cannot be reliably applied at low energies or near the ionization threshold. It is evident from the graphs that the convergence between the present calculations with the experimental data improves as the incident projectile energy increases. By and large, the calculated PICS are within experimental limits beyond 30 eV.

The computation of PICS for $m/z = 15$ was done at 14.56 eV since this energy falls within the energy threshold range available for this ion [73]. Although there are different pathways for the formation of cations having m/z 44, 45, and 50 as indicated by their respective AE thresholds, the relative cation abundances for these cations are the same, implying that at 70 eV, their PICS would be the same. The graphical display presented in Fig. 5b shows that the effect of threshold on PICS is confined to around 50 eV, after which their respective PICS start converging. At 70 eV, the PICS of the fragments having different thresholds are the same. This is in accordance with the mass spectrometry analysis. The TICS obtained in the modified-BEB scheme after summing PICS also agree with the experimental results and the BEB results. This is shown in Fig. 6. The TICS obtained after summing PICS from m-BEB model are slightly lower than BEB-TICS. It is because the experimental channels contribute only 97%. This work demonstrates that a combination of the semiempirical model and the mass spectrometry data can be helpful in providing reliable PICS over an extensive energy range. The calculation is based on the semiempirical formulation of the BEB model.

A shift in the cross section peak is observed in several PICS. This means that the experimental PICS associated with individual reaction channel have energy dependence different from the total cross sections. This indicates a different dynamical mechanism for each dissociative channels just like in the case of methanol and ethanol [76], and WF$_6$ [77]. This results in a different profile for cations. These types of features cannot be reproduced by the present model. This is definitely a limitation of the present model. In such cases, energy-
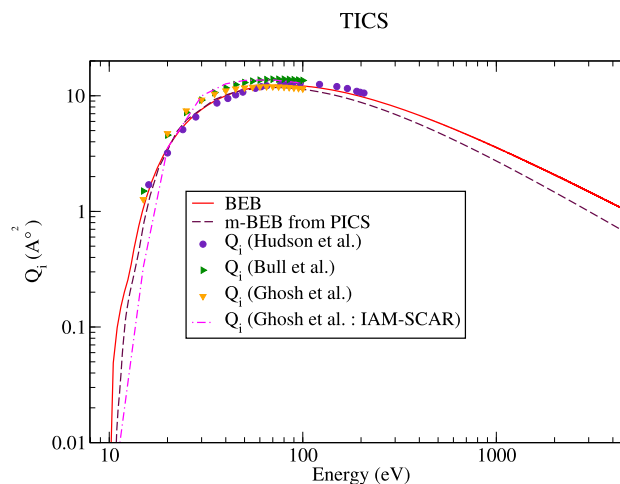
TICS

Fig. 6 "(Color online)" **a** TICS from singly ionized channels: line curve; BEB model, dashed lines; m-BEB results after summing PICS of cations, dotted dashed curve; IAM-SCAR of Ghosh et al. [55], circles; Hudson et al. [81], triangles right; Bull et al. [82], triangles inverted; Ghosh et al. [55]

dependent mass spectrum data may prove useful but this may not be a practical approach. Normally, the electron ionization process is studied at 70 eV. At this incident energy of an electron, fragmentation is spontaneous and stable, and the intensity of ion signals is maximum. A slight variation in the energy of incident electron may not significantly change the fragmentation patterns [56,78]. The electron ionization mass spectrum provides important data to understand the fragmentation of the target molecule and hence gives the relative abundance an important quantity to compute PICS from the BEB model as described earlier. The inability to reproduce experimental peaks satisfactorily is surely a limitation of the present model. But to effectively conclude that this is the reason for cations with $m/z = 12$–15 and 25, additional experi-

mental data are required for investigation. The mass spectrometry data provide a useful insight into the electron impact ionization process. Another advantage of the present model is its simplicity and flexibility. It does not require difficult parameters (differential oscillator strengths) whose non-availability may constitute a bottleneck in the calculations. Kim et al. have used the BEB model but involving a different energy scaling form to compute ionization cross sections for ions [79]. Their cross sections were, however, a little lower than the experimental results. The need to introduce a normalization constant or scaling factor Γ_j arises as the energy scaling term $(t+u+1)$ in the BEB model is not appropriate for ions. The task for determining the correct scaling form becomes easier by using Γ_j. The scaling factor Γ_j normalizes the theoretical BR from m-BEB model to experimental data without affecting the high energy behavior of cross sections. This factor can be easily determined either from the mass spectrometry data or from cross section data and is not unique. Its value is subject to change depending upon the scaling form used. It must be understood that the BEB is only a semiempirical model and its success in predicting TICS is largely due to the energy scaling term. Thus, the scaling is embedded in the BEB model. The use of mass spectrometry data in obtaining Γ_j makes the m-BEB model predictive. The mass spectrometry data are available for many species. It must be noted that in spite of the simplicity of m-BEB model, the agreement between the present and experimental measurements is good, and the differences do not exceed significantly at any energy. This is really remarkable considering the complexity of the precursor molecule. This work establishes that the BEB model can be used to compute PICS of the fragments created during ionization [80].

3 Conclusions

The higher alcohols offer several advantages over fossil fuels. In order to develop biofuels based energy-efficient combustion engines, a better understanding of combustion phenomenon is required. The plasma created due to ignition spark in the internal combustion engines or in other environments can be modeled theoretically, provided a comprehensive electron collision cross section data including those of ions is available. The ions are equally important in any simulation of plasma modeling. Their neglect may violation of charge neutrality in mass diffusion equation thereby leading to inaccurate results. The ionization cross sections are pivotal to understand the mechanism of energy transfer. The mass spectrometry in conjunction with modified-BEB provides a useful insight into the ionization or dissociative ionization process. The attractive feature of the modified-BEB method is that it is easy to implement even for a complex molecule. The results are reliable and also provide an important tool to evaluate the mass spectrometric plasma diagnostics data.

Author contributions

All authors are equally involved in the present work.

Data Availability Statement This manuscript has data included as electronic supplementary material.

Declarations

Conflict of interest The authors declare that they have no known competing financial interests that could have influenced the work reported in this paper.

Data Statement The cross section data of all cations obtained from m-BEB method are provided in the supplementary data sheet.

References

1. N. Gaurav, S. Sivasankari, G.S. Kiran, A. Ninawe, J. Selvin, Renew. Sustain. Energy Rev. **73**, 205 (2017)
2. S. Nanda, P.K. Sarangi, D.-V.N. Vo, *Fuel Processing and Energy Utilization* (CRC Press, 2019)
3. S. Nawab, N. Wang, X. Ma, Y.-X. Huo, Microb. Cell Fact. **19**, 79 (2020)
4. W.R. da Silva Trindade, R.G. dos Santos, Renew. Sustain. Energy Rev. **69**, 642 (2017)
5. A. Atmanli, E. Ileri, B. Yuksel, Energy Convers. Manag. **81**, 312 (2014)
6. J. Han, W. He, L.M.T. Somers, Front Mech. Eng. **6**, 26 (2020)
7. M. Lapuerta, J.J. Hernandez, J. Rodrıguez-Fernandez, J. Barba, A. Ramos, D. Fernandez-Rodrıguez, Int. J Engine Res. **19**(10), 1099 (2018)
8. L. Tipanluisa, N. Fonseca, J. Casanova, J.-M. López, Fuel **302**, 121204 (2021)
9. S.M. Sarathy, M.J. Thomson, C. Togbé, P. Dagaut, F. Halter, C. Mounaim-Rousselle, Combus. Flame **156**, 852 (2009)
10. R.P. Kumar, E. Gnansounou, J.K. Raman, G. Baskar (eds.), *Refining Biomass Residues for Sustainable Energy and Bioproducts* (Academic Press, 2020)
11. Y. Ni, Z. Sun, Appl. Microbiol. Biotechnol. **83**, 415 (2009)
12. J. Čedík, M. Pexa, B. Peterka, M. Müller, M. Holubek, S. Hloch, M. Kucera, Oil Gas Sci Technol. Rev. IFP Energies Nouvelles **76**, 17 (2021)
13. S. Atsumi, T. Hanai, J.C. Liao, Nature **451**, 86 (2008)
14. M. Mascal, Biofuel Bioprod Biorefin. **6**, a483 (2012)
15. S.T. Arnold, A.A. Viggiano, R.A. Morris, J. Phys. Chem. A **102**, 8881 (1998)
16. R.A. Morris, S.T. Arnold, A.A. Viggiano, L.Q. Maurice, C. Carter, E.A. Sutton, Proc. AIAA 2nd Workshop on Weakly Ionized Gases (Norfolk, VA,) (1998)
17. J.B. Heywood, *Internal Combustion Engine Fundamentals* (McGraw-Hill, New York, 1989)
18. A. Starikovskiy, Philos. Trans. R. Soc. A **373**, 20150074 (2015)
19. M.C.A. Lopes, W.A.D. Pires, K.L. Nixon, R.A.A. Amorim et al., Eur. Phys. J. D **74**, 88 (2020)
20. M.J. Brunger, Int. Rev. Phys. Chem. **36**(2), 333 (2017)
21. S.M. Sarathy, S. Vranckx, K. Yasunaga et al., Combust. Flame **159**, 2028 (2012)

22. P. Oßwald, H. Guldenberg, K. Kohse-Hoinghaus, B. Yang, T. Yuan, F. Qi, Combust. Flame **158**, 2 (2011)

23. S.M. Sarathy, P. Oßwald, N. Hansen, K. Kohse-Hoinghaus, Prog. Energy Combust. Sci. **44**, 40 (2014)

24. I. Andersson, L. Eriksson, J. Dyn. Syst. Meas. Control **131** (2009)

25. A. Starikovskiy, N. Aleksandrov, Prog. Energy Combust. Sci. **39**, 61 (2013)

26. I.V. Adamovich, W.R. Lempert, Plasma Phys. Control. Fusion **57**, 014001 (2015)

27. L. Cheng, N. Barleon, B. Cuenot, O. Vermorel, A. Bourdon, Combust. Flame **240**, 111990 (2022)

28. A.C. DeFilippo, J.-Y. Chen, Combust. Flame **172**, 38 (2016)

29. S. Yang, S. Nagaraja, W. Sun, V. Yang, J. Phys. D: Appl. Phys. **50**, 433001 (2017)

30. Y. Ju, W. Sun, Prog. Energy Combust. Sci. **48**, 21 (2015)

31. Y. Ju, J.K. Lefkowitz, C.B. Reuter et al., Plasma Chem. Plasma Process. **36**, 85 (2016)

32. G.J.M. Hagelaar, L.C. Pitchford, Plasma Sour. Sci. Technol. **14**, 722 (2005)

33. S. Mohr, M. Tudorovskaya, M. Hanicinec, J. Tennyson, Atoms **9**, 85 (2021)

34. COMSOL Inc. (2020) https://www.comsol.com/plasma-module

35. P.K. Chu, X. Lu (eds.), *Low Temperature Plasma Technology: Methods and Applications* (CRC Press, 2014)

36. R.E.H. Clark, D.H. Reiter (eds.), *Nuclear Fusion Research: Understanding Plasma-Surface Interactions* (Springer, Berlin, 2005)

37. T.D. MPark, G.H. Dunn (eds.), *Electron Impact Ionization* (Springer, 1985)

38. T. Makabe, Z. Lj, *Petrović, Plasma Electronics: Applications in Microelectronic Device Fabrication*, 2nd edn. (CRC Press, Boca Raton, 2015)

39. R.K. Janev (ed.), *Atomic and Molecular Processes in Fusion Edge Plasmas* (Springer, Boston, 1995)

40. P. Oßwald, M. Kohler, Rev. Sci. Instrum. **86**, 105109 (2015)

41. A. Lucassen, N. Labbe, P.R. Westmoreland, K. Kohse-Höinghaus, Combust. Flame **158**, 1647 (2011)

42. N. Hansen, T.A. Cool, P.R. Westmoreland, K. Kohse-Höinghaus, Prog. Energy Combust. Sci. **35**, 168 (2009)

43. B. Chen, H. Wang, Z. Wang, J. Han, A.B.S. Alquaity, H. Wang, N. Hansen, S.M. Sarathy, Combust. Flame **202**, 208 (2019)

44. S.E. Huber, A. Mauracher, D. Süß, I. Sukuba et al., J. Chem. Phys. **150**, 024306 (2019)

45. M.C. Fuss, A.G. Sanz, A. Munoz, F. Blanco, M.J. Brunger, S.J. Buckman, P. Limao-Vieira, G. García, Appl. Radiat. Isotopes **83**, 159 (2014)

46. M.U. Bug, W.Y. Baek, H. Rabus, C. Villagrasa, S. Meylan, A.B. Rosenfeld, Radiat. Phys. Chem. **130**, 450 (2017)

47. L. Campbell, M.J. Brunger, Plasma Sour. Sci. Technol. **22**, 013002 (2013)

48. M.J. Brunger, Int. Rev. Phys. Chem. **35**(2), 297 (2016)

49. I. El Naqa, P. Pater, J. Seuntjens, Phys. Med. Biol. **57**, R75 (2012)

50. L.C. Pitchford, L.L. Alves, K. Bartschat et al., Plasma Process. Polym. **14**, 1600098 (2017)

51. M.A. Ridenti, J.A. Filho, M.J. Brunger, R.F. da Costa et al., Eur. Phys. J. D **70**, 16 (2016)

52. W.M. Huo, Y.-K. Kim, I.E.E.E. Trans, I.E.E.E. Trans, Plasma Sci. **27**(5), 1225 (1999))

53. J.S. Yoon, M.-Y. Song, H. Kato et al., J. Phys. Chem. Ref. Data **39**, 033106 (2010)

54. A. Bharadvaja, S. Kaur, K.L. Baluja, Eur. Phys. J. D **73**, 251 (2019)

55. S. Ghosh, K.L. Nixon, W.A.D. Pires, R.A.A. Amorim et al., Int. J. Mass. Spectrom. **430**, 44 (2018)

56. W.A.D. Pires, K.L. Nixon, S. Ghosh, R.A.A. Amorim et al., Int. J. Mass. Spectrom. **430**, 158 (2018)

57. A.N. Zavilopulo, F.F. Chipev, L.M. Kokhtych, Nucl. Instrum. Methods Phys. Res. B **233**, 302 (2005)

58. A.S. Kadyrov, I. Bray, J. Phys. B: At. Mol. Opt. Phys. **49**, 222002 (2016)

59. I. Bray, D.V. Fursa, A.S. Kheifets, A.T. Stelbovics, J. Phys. B: At. Mol. Opt. Phys. **35**, R117 (2002)

60. I. Bray, D.V. Fursa, A.S. Kadyrov, A.T. Stelbovics, A.S. Kheifets, A.M. Mukhamedzhanov, Phys. Rep. **520**, 135 (2012)

61. P.K. Biswas, J.S.E. Germano, T. Frederico, J. Phys. B: At. Mol. Opt. Phys. **35**, L409 (2002)

62. M.C. Zammit, D.V. Fursa, J.S. Savage, I. Bray, J. Phys. B: At. Mol. Opt. Phys. **50**, 123001 (2017)

63. N.A. Mori, R. Utamuratov, L.H. Scarlett, D.V. Fursa, A.S. Kadyrov, I. Bray, M.C. Zammit, J. Phys. B: At. Mol. Opt. Phys. **53**, 105203 (2020)

64. I. Bray, I.B. Abdurakhmanov, J.J. Bailey et al., J. Phys. B: At. Mol. Opt. Phys. **50**, 202001 (2017)

65. J.R. Hamilton, J. Tennyson, S. Huang, M.J. Kushner, Plasma Sour. Sci. Technol. **26**, 065010 (2017)

66. A. Bharadvaja, M. Bassi, A.K. Arora, K.L. Baluja, Plasma Sour. Sci. Technol. **30**, 095012 (2021)

67. K. Goswami, A.K. Arora, A. Bharadvaja, K.L. Baluja, Eur. Phys. J. D **75**, 228 (2021)

68. A.K. Arora, K.K. Gupta, K. Goswami, A. Bharadvaja, K.L. Baluja, Plasma Sour. Sci. Technol. **31**, 015008 (2022)

69. Y. Kumar, M. Kumar, Chem. Phys. Lett. **740**, 137071 (2020)

70. Y.-K. Kim, M.E. Rudd, Phys. Rev. A **50**, 3954 (1994)

71. J.P. Santos, F. Parente, Y.-K. Kim, J. Phys. B **36**(21), 4211 (2003)

72. GAUSSIAN 03 (Gaussian, Inc., Wallingford, CT. 2003)

73. https://webbook.nist.gov/chemistry/

74. R.A. Friedel, J.L. Shultz, A.G. Sharkey, Anal. Chem. **28**, 926 (1956)

75. W.A.D. Pires, K.L. Nixon, S. Ghosh, R.F.C. Neves et al., Int. J. Mass Spectrom. **422**, 32 (2017)

76. K.L. Nixon, W.A. Pires et al., Int. J. Mass Spectrom. **404**, 48 (2016)

77. R. Basner, M. Schmidt, K. Becker, Int. J. Mass Spectrom. **233**, 25 (2004)

78. K.K. Irikura, J. Chem. Phys. **145**, 224102 (2016)

79. K.K. Irikura, Y.-K. Kim, M.A. Ali, J. Res. Natl. Inst. Stand. Technol. **107**, 63 (2002)

80. K. Fedus, G.P. Karwasz, Eur. Phys. J. D **71**, 138 (2017)

81. J.E. Hudson, M.L. Hamilton, C. Vallance, P.W. Harland, Phys. Chem. Chem. Phys. **5**, 3162 (2003)

82. J.N. Bull, P.W. Harland, C. Vallance, J. Phys. Chem. A **116**, 767 (2012)